

PCCP

Accepted Manuscript



This is an *Accepted Manuscript*, which has been through the Royal Society of Chemistry peer review process and has been accepted for publication.

Accepted Manuscripts are published online shortly after acceptance, before technical editing, formatting and proof reading. Using this free service, authors can make their results available to the community, in citable form, before we publish the edited article. We will replace this *Accepted Manuscript* with the edited and formatted *Advance Article* as soon as it is available.

You can find more information about *Accepted Manuscripts* in the [Information for Authors](#).

Please note that technical editing may introduce minor changes to the text and/or graphics, which may alter content. The journal's standard [Terms & Conditions](#) and the [Ethical guidelines](#) still apply. In no event shall the Royal Society of Chemistry be held responsible for any errors or omissions in this *Accepted Manuscript* or any consequences arising from the use of any information it contains.

**Alternative Alcohol-soluble Conjugated Small Molecule Electrolytes for
High-efficiency Inverted Polymer Solar Cells**

Yueqin Shi¹, Licheng Tan^{1,2}, Lie Chen^{1,2}, Yiwang Chen^{*1,2}

¹School of Materials Science and Engineering/Institute of Polymers, Nanchang University, 999 Xuefu Avenue, Nanchang 330031, China; ²Jiangxi Provincial Key Laboratory of New Energy Chemistry, College of Chemistry, Nanchang University, 999 Xuefu Avenue, Nanchang 330031, China

Abstract:

New alcohol-soluble conjugated small molecule electrolytes (CSMEs), 3,6-bis-(5-benzoic acid-thiophen-2-yl)-2,5-bis-(2-ethylhexyl)-2,5-dihydro-pyrrolo[3,4-*c*]pyrrole-1,4-dione liquid crystalline (DPP-COOH) and di-tetrabutylammonium cis-bis(isothiocyanato)bis(2,2'-bipyridyl-4,4'-dicarboxylato) ruthenium (II) dye (N719), are developed as interfacial modification in inverted polymer solar cells (PSCs). Further optimization of the device architecture by combining the electrolytes as hole and electron buffer layers can significantly promote the photovoltaic performances of PSCs due to the integrated advantages of excellent alcohol processibility, hole and electron mobility, interfacial dipole effect and well energy level alignment with electrodes. Moreover, the PSCs with the CSMEs interlayers based on narrow band gap PTB7:PC₇₁BM active layer show considerable improvement in power conversion efficiency (PCE), compared with P3HT:PCBM active layer-based devices. Devices with DPP-COOH and N719 modifications after thermal treatment at 120 °C exhibit the PCE of 8.0% and 7.6% under AM 1.5G irradiation respectively, improving from 6.7% PCE of the pristine device without any interfacial layer. Encouragingly, the use of CSMEs as hole and electron modification layers simultaneously can boost the PCE to 8.2%. These findings demonstrate the utilization of alcohol-soluble small molecule conjugated electrolyte with lower band gap as interfacial modification layers is an effective and practical strategy to improve

* Corresponding author. Tel.: +86 791 83968703; fax: +86 791 83969561. *E-mail address:* ywchen@ncu.edu.cn (Y. Chen).

photovoltaic performance in PSCs.

Keywords: alcohol-solubility; conjugated electrolytes; carrier mobility; polymer solar cells

Introduction

Bulk heterojunction (BHJ) solar cells^[1-3] comprising conjugated polymer donor and fullerene acceptor have attracted a great deal of interest for their promising advantages including low cost, lightweight, flexibility and large-scale fabrication through roll-to-roll process. Recently, power conversion efficiencies (PCEs) of BHJ solar cells have been optimized by development of new conjugated polymer donors or new fullerene-derived acceptors, nanoscale morphology control and optimization of device structures.^[3-6] Besides, in order to be competitive with conventional photovoltaic technologies based on silicon or other inorganic materials, the efficiency, lifetime and solution processing of BHJ solar cells still need to be significantly improved.

The photovoltaic effect involves generation of electrons and holes in the BHJ solar cells device under illumination, and subsequent charge collection at corresponding electrodes. Photon absorption of organic optoelectronic materials often creates bound electron-hole pairs (excitons). Charge collection at corresponding electrodes, requires dissociation of the excitons, which occurs only at the heterojunction interface between conjugated polymer donor materials and acceptor materials with different ionization potentials or electron affinities. In addition to new active layer materials' design^[7] and morphology optimization of the donor/acceptor interface^[8-11], interface engineering^[12-14] on BHJ solar cells device was of great importance in regulating the efficiency of charge separation and charge collection, and hence, enhancing the power conversion efficiency (PCE) and device stability.

To improve the charge selectivity transmission and collection, and minimize the energy barrier for charge extraction at electrodes, the work function (WF) of hole-transporting layer (HTL) with electron-blocking properties need to match the highest occupied molecular orbital (HOMO) level of donor and the WF of

electron-transporting layer (ETL) with hole-blocking properties should match the lowest unoccupied molecular orbital (LUMO) level of acceptor in the active layer, respectively. Therefore, HTL between anode and active layer, as well as ETL between cathode and active layer, is essential for achieving maximum BHJ device efficiency and lifetime. The functions of hole and electron interfacial layers (ILs) include: a) to minimize the energy barrier for charge extraction; b) to selectively extract one sort of charge carriers and block the opposite charge carriers; c) to improve the interface stability between the electrode and the active layer; d) to modify the surface property and alter the active layer morphology; e) to form the interfacial dipole for energy level alignment.

Recently, HTL layers contain several classes of materials, including highly doped polymer PEDOT:PSS, self-assembled monolayers, 3,3,3-trifluoropropyltrichlorosilane, metal oxide inorganic semiconductors (such as, MoO₃, V₂O₅, WO₃, NiO), graphene-based materials and conjugated polyelectrolytes (CPEs).^[15-16] On the other hand, the materials used as ETL include low WF metals or related salts (e.g. Ca, LiF), metal oxide semiconductors (e.g. TiO₂, ZnO) and fullerene derivatives. Besides, for the advantages of reducing series resistance, increasing internal built-in voltage, and modification of the electron extraction properties, the CPEs ETL have recently received increasing attention with the proven ability of improving PCE through solution processing and given the record high device efficiency.^[17-19] However, the function of CPEs in affecting the hole injection/extraction has been rarely addressed. One reason is that directly depositing CPEs on top of ITO substrate can often lead to decrease the WF of electrode due to interfacial dipole interaction, resulting in hole extraction barrier. Another limitation is that most CPEs show relatively low electrical conductivity, as demonstrated by Bazan *et al.*^[13]

It was well-known that diketopyrrolopyrrole (DPP)-based conjugated small molecules and polymeric materials have been demonstrated to render high hole or electron transporting motilities and photovoltaic properties.^[20-22] Reynolds *et al.* had synthesized amphiphilic self-assembled diketopyrrolopyrrole-based oligothiophenes

and investigated its semiconductive properties in field-effect transistors and solar cells.^[23] Conjugated small molecule electrolytes (CSMEs) are also neutral, hydrophilic, electrical molecules, which are attractive for achieving the beneficial properties of CPEs (alcohol solubility; pendent dipoles). However, to the best of our knowledge, CSMEs have not been tested for their ability as the IL in BHJ solar cells.

Herein, we synthesized phenylthiophene-appended DPP, 3,6-bis-(5- benzoic acid-thiophen-2-yl)-2,5-bis-(2-ethylhexyl)-2,5-dihydro-pyrrolo[3,4-*c*]pyrrole-1,4-dione (DPP-COOH) conjugated small molecule and first utilized it as IL in device fabrication. DPP-COOH was designed as the low band-gap π -conjugated core and was tethered with carboxylic acid groups, which enhance solubility and film-forming properties. It provided a novel way to improve the photovoltaic performance with the CSMEs as ILs, especially as ETL for its high charge carrier mobility and interfacial dipole effect. Meanwhile, a dye molecule di-tetrabutylammonium cis-bis(isothiocyanato)bis(2,2'-bipyridyl-4,4'-dicarboxylato)ruthenium (II) (N719) with the similar energy level and polarity carboxylic acid groups was also used to further testify the enhancement of efficiency and stability of BHJ solar cells when inserting the CSMEs into BHJ solar cells devices. By casting DPP-COOH and N719 onto active layer surface as HTL or the ZnO thin film surface as ETL, the PCE increasing from 6.7% (pristine device without any IL) to 7.6%, 7.2% (HTL) and 8.0%, 7.6% (ETL) under AM 1.5G irradiation was achieved for cells with inverted structure, respectively. The excellent photovoltaic properties with CSMEs as ILs may be based on the following reasons: minimizing the energy barrier for charge transportation and extraction; improving the interface stability between the electrode and active layer; modifying the surface property and decreasing the interfacial defect of MoO₃ and ZnO; altering the active layer morphology and forming the interfacial dipole for energy level alignment. Combining the advantages of them as HTL and ETL, the device with DPP-COOH as HTL and ETL simultaneously showed the best PCE of 8.2%.

Results and Discussion

Simple diketopyrrolopyrrole (DPP)-based small molecule, DPP-COOH was first synthesized by using palladium-catalyzed Suzuki-Miyaura cross-coupling reaction in **Scheme S1**. To make this small molecule with a more appropriate energy level alignment with MoO₃/Ag anode relatively, the phenylthiophene-appended DPP was designed as the low bandgap π -conjugated core. Besides, the carboxylic acid groups were tethered with this core to enhance solubility in alcohol solvent and film-forming properties in device fabrication. And DPP class with high hole and electron mobility was a good requirement for obtaining excellent photovoltaic performance to ensure effective charge carrier transport to the electrodes and reduce the photocurrent loss in the BHJ solar cells.^[24-27] The kinked DPP-COOH backbone-induced packing architecture offered a fascinating new set of structural parameters to be tuned in the quest for BHJ device structures that could maximize the PCE of device. As expected, DPP-COOH was soluble in alcohol solvent, such as methanol, ethanol, etc. Besides, the improvement in device performance originated from the morphological optimization and alteration of electronic energy level alignment at the heterointerfaces, especially for the dipole formation at the interface of the active layer and metal electrode.^[28] Hence, DPP-COOH and N719 with the similar energy level and polarity carboxylic acid groups as HTL and ETL, respectively, were used as the hole and electron ILs to optimize the device performance in **Scheme 1**. In order to investigate the effect of morphologies on photovoltaic properties, the molecular orientation and liquid crystalline organization of DPP-COOH thin film under thermal annealing was explored by polarized optical microscopy (POM) and differential scanning calorimetry (DSC), shown in **Fig. 1**. With increasing annealing temperature, the emergence of highly birefringent liquid crystalline domains with sizes over several hundreds of nanometers from POM images, indicated that the spontaneous formation of well-assembly crystallites within this film at 120 °C thermal annealing. The molecular orientation nano-structure might be conducive to exciton dissociation and charge collection at electrode. Therefore, selection of 120 °C would be considered as appropriate thermal treatment temperature for devices with CSMEs as ILs. The UV/vis absorption spectra of DPP-COOH and N719 spin-casted from methanol

solution (**Fig. 1**) presented the absorption peaks (λ_{max}) at 368 nm, 650 nm for DPP-COOH and 317 nm, 390 nm, 550 nm for N719. The wide absorption peak at 650 nm for DPP-COOH corresponded to the π - π^* (HOMO-LUMO) transition, which was likely intrinsic to the single molecule with restricted intra-molecular motion. The absorption bands of these small molecules extended from 300 nm to a lower energy level of \sim 800 nm in the films, and the optical band gap of DPP-COOH and N719 were estimated to be 1.55 eV and 1.86 eV from the absorption edge. The HOMO energy levels of DPP-COOH and N719 films had been determined to be -5.47 eV and -5.05 eV approximately.

The nano-morphology of HTLs deposited on top of active layer can significantly further affect the charge transport and collection in corresponding electrode. To examine the impact of active layer on the morphology of DPP-COOH and N719 interlayers, we measured pristine morphology of CSMEs first. **Fig. S1** showed the tapping-mode atomic force microscopy (AFM) high and phase images of CSMEs spin-coating onto ITO substrates with and without thermal annealing at 120 °C for 10 min. The DPP-COOH film showed many crystalline domains and relative smooth surface with a root-mean-square (RMS) roughness of 1.63 nm, while N719 exhibited typical tiny and dense cluster nanostructure with a RMS roughness of 2.39 nm. After thermal annealing, the crystalline regions of DPP-COOH grew up to larger size (100 nm-500 nm) and the RMS roughness increased to 20.5 nm, which was in favor of enhancing the interfacial areas between active layer and corresponding electrode^[29]. However, the film of N719 showed a fine-distribution and denser of polarity molecules cluster with a RMS roughness of 3.12 nm.

The AFM measurements were also carried out to further investigate the influence of active layer on the nano-morphology spontaneous formation of the well-organized DPP-COOH liquid crystalline molecule and N719 dye molecule in **Fig. S2**. The high and phase images of pristine P3HT:PCBM active layer illustrated nanoscale phase separation and a smooth surface morphology with a RMS roughness of 1.32 nm, which could enable a large interface area for exciton dissociation. After spin-coating CSMEs onto the active layer surface, then we further measured the surface

morphology of P3HT:PCBM/DPP-COOH and P3HT:PCBM/N719 films with and without thermal annealing at 120 °C for 10 min. All the films displayed similar nanoscale phase-separated morphologies. Compared with the film without thermal annealing, P3HT:PCBM/DPP-COOH film showed RMS roughness from 3.31 nm to 5.16 nm and had an orientation crystalline nanostructure with higher molecular order after thermal annealing, providing a better pathway for the transportation of generated charge carriers. P3HT:PCBM/N719 film showed RMS roughness from 2.46 nm to 3.51 nm and had a denser cluster nanostructure. The roughness surfaces implied the better interfacial adhesion between HTL and MoO₃ layer, consequently a better charge transport.^[30]

The photovoltaic performances of the devices based on the CSMEs as HTLs were quite sensitive to the CSMEs' morphologies. Therefore, the morphology of DPP-COOH liquid crystalline and N719 dye molecules as HTL affected by the active layer was further investigated by transmission electron microscopy (TEM) in **Fig. 1**. After CSMEs were spin-coated onto the active layer surface as HTLs with thermal annealing at 120 °C, more orderly nano-morphologies could be observed. The N719 dye molecule clusters in nanoscales were well-dispersed and DPP-COOH liquid crystalline nanofibrils presented high crystalline orientation on the surface of active layer, which could be beneficial for charge transport and collection at anode. Meanwhile, the crystalline orientation and orderly structure of DPP-COOH on active layer could yield better carriers transport channel with respect to N719, which can be in favor of high J_{sc} and FF of the device.

Ultraviolet photoelectron spectroscopy (UPS) was utilized to characterize the intrinsic electronic characteristics of the polymer-metal interfaces in films. As HTLs, CSMEs were spin-coated between active layer and MoO₃ layer. In order to verify the effect of CSMEs on MoO₃ thin layer, ultraviolet photoelectron spectroscopy (UPS) was carried out to study the energy levels of MoO₃, DPP-COOH/MoO₃ and N719/MoO₃ thin layers. Observing from **Fig. S3**, the WF for MoO₃, DPP-COOH/MoO₃ and N719/MoO₃ thin layers were determined to be approximately -5.53 eV, -5.27 eV and -4.99 eV respectively, summarizing in **Fig. 2**. The different in WF ($\delta\Phi_{AC}$) between the

anode (Ag) and cathode induced a potential gradient across the active layer. The CSMEs interlayers that reduced the WF (negative interfacial dipole (Δ)) at the anode interface decrease $\delta\Phi_{AC}$ and thus reduced V_{oc} , which was consistent with the devices' data. The dipole orientation of the device architecture with CSMEs as HTLs was downward. Besides, the CSMEs as HTLs induce a larger interfacial dipoles with anode electrode, with the interfacial dipole energy Δ as high as 1.2 eV and 0.5 eV for N719 and DPP-COOH respectively, resulting in the formation of hole extraction barrier. Moreover, the WF of DPP-COOH/MoO₃ (-5.27 eV) displayed more appropriate with the HOMO of donor materials than that of N719/MoO₃ (-4.99 eV). However, several other factors must be considered when using the CSMEs as HTLs, the potential to directly contribute to the photocurrent within the device and the charge mobility of the device with these HTLs.

The CSMEs as HTLs between the P3HT:PCBM active layer and MoO₃ played an important role in the performance of inverted single-junction solar cells in **Fig. S4**. It was imperative to optimize the device structure to improve the power conversation efficiency (PCE) of the inverted BHJ solar cells. The optimal thickness of MoO₃ was found to be around 6 nm as measured by J - V measurements. Without the CSMEs layer, inverted BHJ solar cells showed short-circuit current (J_{sc}) of 8.31 mA/cm², open-circuit voltage (V_{oc}) of 0.59 V, fill factor (FF) of 59% and corresponding PCE of 2.9%. After inserting CSMEs between active layer and MoO₃, inverted device with DPP-COOH layer showed the photovoltaic performance from J_{sc} of 8.92 mA/cm², V_{oc} of 0.59 V, FF of 48%, PCE of 2.6% to J_{sc} of 8.86 mA/cm², V_{oc} of 0.58 V, FF of 57%, corresponding PCE of 3.0% after thermal annealing, while the device with N719 layer from J_{sc} of 10.47 mA/cm², V_{oc} of 0.57 V, FF of 50%, PCE of 2.9% to J_{sc} of 9.24 mA/cm², V_{oc} of 0.58 V, FF of 58%, corresponding PCE of 3.1% after thermal annealing. The V_{oc} of 0.58 V or 0.57 V from the inverted BHJ solar cells with CSMEs were lower than the V_{oc} of 0.59 V from the cells without ILs, which was due to the lower $\delta\Phi_{AC}$ in inverted BHJ solar cells. This observation was in good agreement with the band alignment from UPS results. On the other hand, the larger J_{sc} of the devices with CSMEs layer arose from the stronger light absorption intensity (UV-vis

absorption spectra and IPCE response), higher hole-mobility based on the SCLC results (**Supporting Information**), and enhanced contact between active layer and anode because of amphiphilic property of CSMEs. The device performance parameters are summarized in **Table 1**. The devices with N719 as IL between active layer and MoO₃ possessed stronger light absorption, resulting in better J_{sc} , probably due to cluster N719 acting as an ‘optical spacer’ for the redistribution of an optical field in the active layer.^[31]

To evaluate the suitability of the newly developed CSMEs as HTL, PSCs were fabricated with PTB7:PC₇₁BM active layer to further testify the potentially interfacial engineering for obtaining high performance BHJ solar cells.^[24] The J - V curves of the cells with appropriate lower-band-gap active layer were presented in **Fig. S5**, and detailed data for V_{oc} , J_{sc} , FF and PCE were included in **Table 1**. The PCE of device without CSMEs layer is 6.7% (V_{oc} of 0.72 V, J_{sc} of 14.6 mA/cm², and FF of 64%), comparable to the referred value.^[24] After optimizing the interface of oil-soluble active layer and polar inorganic metal oxides with amphiphilic CSMEs layer, the devices with N719 and DPP-COOH layers showed a drastically enhancement of photovoltaic performances with the best PCE of 7.2% (V_{oc} of 0.72 V, J_{sc} of 16.76 mA/cm², and FF of 60%) and 7.6% (V_{oc} of 0.72 V, J_{sc} of 16.24 mA/cm², and FF of 65%) after thermal treatment, respectively. Compared to pristine cell, the devices with CSMEs showed the significant increase of J_{sc} and slight reduction of V_{oc} . The donor polymer of narrow band-gap PTB7:PC₇₁BM active layer had deeper HOMO level than that of P3HT:PC₆₁BM active layer. The relative less WF reduction of DPP-COOH/MoO₃ as HTL resulted in more suitable selection for interfacial modification with narrow band-gap PTB7:PC₇₁BM active layer in comparison with N719/MoO₃ as HTL. In fact, the PCE results of devices confirmed the above evidence.

Generally CSMEs ILs as ETL in photovoltaic devices have been reported. We rationalized that the utilization of alcohol-soluble CSMEs as anode ILs could offer a new strategy to improve the photovoltaic performance of device, which displayed great potential in the practical applications, especially for the fabrication of

environmental-friendly device. A second type of device with CSMEs as ETL on the surface of ZnO was processed to probe the influences by the interfacial dipoles alignment of CSMEs on photovoltaic properties. UPS measurement was also employed to further probe the electronic properties of CSMEs as ETL in **Fig. S6**, which could enable an evaluation of the energy level of ZnO, as well as Δ values of the interface between ZnO and active layer. The Δ is calculated as the difference in measured E_{SEC} values of the film (N719/ZnO or DPP-COOH/ZnO) and pristine ZnO film.^[32] The HOMO energy levels for ZnO, ZnO/DPP-COOH and ZnO/N719 thin layers were calculated as -7.75 eV, -7.62 eV and -7.52 eV. Based on these HOMO energies and optical gaps obtained from the onset of absorption spectra, the estimated LUMO energy levels for ZnO, ZnO/DPP-COOH and ZnO/N719 thin layers were -4.46 eV, -4.28 eV and -4.09 eV, respectively. The difference of energy levels among pristine ZnO, ZnO/N719 and ZnO/DPP-COOH, implied that the energy levels of ZnO could be tuned by the CSMEs. Most importantly, these energy differences indicated that the well band alignment of inverted BHJ solar cells with CSMEs, especially for the device based on PTB7:PC₇₁BM active layer, compared with the device without ILs (**Fig. 2**). Hence, a large V_{oc} from the inverted BHJ solar cells with CSMEs was anticipated. Besides, the built-in electric field in the BHJ layer induced by ZnO/N719 and ZnO/DPP-COOH ETLs was enhanced, deriving from the adverse Δ with built-in electric field^[33], which could promote exciton dissociation, increase photogenerated-carrier collection and J_{sc} of the device. Furthermore, the advantage of CSMEs as ETL also lied in their ability to produce large Δ with anode electrode, which could form a better contact between the active layer and ZnO layer.

The space charge-limited-current (SCLC) model (**Fig. S7**) was further used to investigate carrier mobility of CSMEs modification in the device. Furthermore, as the enhancement in photovoltaic properties can also be related to the charge transport and collection, the impact of CSMEs on charge carrier mobilities had also been assessed in BHJ solar cells. The built-in electric field in the BHJ layer induced by CSMEs as ETLs was expected to promote exciton dissociation and increase photogenerated-carrier collection.^[34] However, the reverse built-in electric field in the

BHJ layer induced by CSMEs as HTLs resulted in the formation of hole extraction barrier. In order to evaluate the apparent charge carrier mobility in the active layer, $J^{0.5}$ - V characteristics of single charge carrier devices were measured using SCLC according to the Mott-Gurney equation (details of the mobility measurement is described in **Supporting Information**).^[35-39] As plotted in **Fig. S7** and summarized in **Table S1**, the apparent electron mobility of the devices increased from $2.94 \times 10^{-3} \text{ cm}^2 \text{ V}^{-1} \text{ s}^{-1}$ to $3.55 \times 10^{-3} \text{ cm}^2 \text{ V}^{-1} \text{ s}^{-1}$ and $4.16 \times 10^{-3} \text{ cm}^2 \text{ V}^{-1} \text{ s}^{-1}$, and hole mobility $2.74 \times 10^{-4} \text{ cm}^2 \text{ V}^{-1} \text{ s}^{-1}$ to $4.92 \times 10^{-4} \text{ cm}^2 \text{ V}^{-1} \text{ s}^{-1}$ and 4.01×10^{-4} after insertion of N719 and DPP-COOH ILs into devices, respectively. The results revealed that the incorporation of CSMEs into the ILs could achieve the increase of both electron-mobility and hole-mobility (the dual carrier mobility) and more balanced charge transport in the devices. Besides, the inserting of CSMEs modification could avoid the current leakage and decrease bias-dependent carrier recombination, subsequently yielding the increased J_{sc} and FF of the device (J - V characteristics under dark condition), comparing with devices without ILs.

It was well-known that the difference self-assembly architecture of ETLs resulted in various organization of the active layer nanostructures. The orientation and accumulation of CSMEs on the surface of ZnO was investigated by X-ray photoelectron spectroscopy (XPS) and atomic force microscopy (AFM) measurements. From the XPS peaks in **Fig. S8**, one peak at 1021.1 eV corresponding to Zn 2p 3/2 for Zn-O bonds in ZnO was observed, while there were two peaks displaying in ZnO/N719 and ZnO/DPP-COOH at 1021.1 eV and 1021.3 eV respectively, revealing the self-assembly of CSMEs driven by the potential interaction between ZnO and CSMEs. On the other hand, the binding energy at 530.1 eV (low-binding-energy) is attributed to the O 1s level in the stoichiometric ZnO structure, bonding to Zn atoms. The binding energy at 531.4 eV (high-binding-energy) is associated with the surface being deficient in O 1s, such as the O 1s in zinc hydroxide, Zn(OH)₂, or the oxygen species adsorbed by the surface hydroxyl groups.^[40] In addition, the intensity of the high-binding-energy oxygen atoms was significantly reduced with the modification of CSMEs, indicating the

oxygen-deficiency of ZnO/N719 and ZnO/DPP-COOH could be passivated to offer close contact with active layer and an efficient path for electron transport.^[41] The surface topographies of pristine ZnO, ZnO/N719 and ZnO/DPP-COOH were further investigated by AFM and the correlative results were shown in **Fig. S9** and **Fig. 3**. Compared with pristine ZnO with RMS roughness of 1.63 nm, the surface of the films became larger roughness of 2.27 nm and 2.05 nm without thermal annealing and relative smoother of 2.0 nm and 1.47 nm after modification with N719 and DPP-COOH CSMEs with thermal annealing at 120 °C for 10 min. The larger roughness structure, satisfying the requirement of the device performance, increased the surface area of CSMEs vastly and benefited the contact with active layer by enhancing the partial permeation of active layer. After spin-coating the active layer P3HT:PCBM and PTB7:PC₇₁BM onto the surface of ETLs, AFM was also carried out to test the influence of CSMEs layer on the active layer morphology. Compared with the surface roughness of P3HT:PCBM on pristine ZnO thin film (RMS:1.32 nm), the surface roughness of P3HT:PCBM on ZnO/N719 and ZnO/DPP-COOH thin films were 1.07 and 1.17 nm without annealing, 0.88 nm and 0.77 nm with thermal annealing treatments at 120 °C for 10 min. The smoother surface of active layer might attribute to the better interfacial adhesion between active layer and ZnO and the good partial permeation of active layer, especially for the DPP-COOH modification thin films, which is consistent with the results with PTB7:PC₇₁BM active layer (**Fig. 3**). Besides, the much fine pattern of the film with DPP-COOH modification than it with N719 annealing at 120 °C could be observed, suggesting more intimate interface between ZnO and PTB7:PC₇₁BM active layer, which might be the structural similarity of DPP-COOH and active layer material.

Current density-voltage (J - V) characteristics of P3HT:PCBM and PTB7:PC₇₁BM solar cells with CSMEs as ETL were displayed in **Fig. S10** and **Fig. S11**, and the detailed device parameters were shown in **Table 2**. The performances of the devices with CSMEs were improved with larger J_{sc} , better V_{oc} and slightly better FF, especially for the devices with CSMEs modification and thermal annealing treatments, compared to the device without IL. The slight increase in V_{oc} (from 0.72 V to 0.73 V

or 0.74 V) could be ascribed to the better energy level alignments of devices and the CSMEs chains forming an interfacial dipole moment with its negative pole pointing towards the ZnO, which could increase the HOMO and LUMO levels of the active layer. An increase of IPCE at wavelengths from 300 nm to 800 nm and the enhance of built-in electric field originated from the inversed interfacial dipole were also observed after inserting CSMEs, which led to the J_{sc} of pristine device without any ILs changed from 14.6 mA/cm² to 15.44 mA/cm² (without annealing) and 16.01 mA/cm² (thermal annealing) for the devices with DPP-COOH layer, and to 15.29 mA/cm² (without annealing) and 15.92 mA/cm² (thermal annealing) for the devices with N719 layer. Finally, 7.6 % and 8.0% of PCE with N719 and DPP-COOH (thermal annealing) as ETLs were obtained. The maximum IPCE with IL was over 70%, indicative of efficient photon-to-electron conversion. Besides, $J-V$ characteristics under dark condition indicated that good diode characteristics were obtained from both devices using CSMEs as ETLs (**Fig. S12**). As a result, the energy barrier for electron injection and collection could be reduced. All data were consistent with results with P3HT:PCBM active layer in **Fig. S10**. Moreover, the lower band-gap PTB7:PC₇₁BM with amphiphilic CSMEs ILs increased the device performance much better with relative to P3HT:PCBM active layer due to the better energy alignment of device (**Fig. 2**).

Combining the advantages of CSMEs as HTL and ETL, the devices with CSMEs as HTL and ETL simultaneously were fabricated to further boost the inherent performance, resulting in a considerable gain in overall photovoltaic output and yielding the best PCE of 8.2% for the device with DPP-COOH ILs. The enhanced performance could be explained by a larger $\delta\Phi_{AC}$, stronger built-in electric field, redistribution of an optical field in the active layer, interfacial modification between active layer and corresponding electrodes for the amphiphilic properties of the CSMEs and the higher carrier mobility after inserting the CSMEs. All device parameters based on PTB7:PC₇₁BM active layers with various optimizing structures were summarized in **Fig. 4**. Expect for the device efficiency improvement, enhanced device stability from the optimized interfacial layers was also observed in **Fig. S13**.

So the amphiphilic CSMEs with low bandgap π -conjugated core and the carboxylic acid groups as ILs were proved to be a good way to slow down the degradation of devices.

Conclusions

Through the interfacial modification by the novel low band-gap CSMEs DPP-COOH and N719, the higher efficiency inverted PSC have been achieved, especially for the device based on PTB7:PC₇₁BM active layer. Comparing with the N719, the self-assembled DPP-COOH as IL reveals better photovoltaic performance due to its highly orientation of nanofiber morphology, more appropriate energy level alignment of the device and relative good hole and electron carrier mobility. The PCE of device without CSMEs layer is 6.7% (V_{oc} of 0.72 V, J_{sc} of 14.6 mA/cm², and FF of 64%). As HTL of CSMEs, the devices with N719 and DPP-COOH layers were further improved with the best PCE of 7.2% (V_{oc} of 0.72 V, J_{sc} of 16.76 mA/cm², and FF of 60%) and 7.6% (V_{oc} of 0.72 V, J_{sc} of 16.24 mA/cm², and FF of 65%) after thermal treatment, respectively. The enhanced performance is attributed to the highly hole carrier mobility, orderly transport channel and the redistribution of an optical field in the active layer with amphiphilic CSMEs as HTL. On the other hand, as ETL of CSMEs, 7.6 % and 8.0% of PCE with N719 and DPP-COOH after annealing at 120 °C were obtained for the PSCs, due to its interfacial dipole effect, excellent electron mobility and better energy level alignments of devices. Further optimization of the device architecture, 8.2% of the best PCE was achieved when using DPP-COOH as hole and electron modification layers simultaneously. Moreover, the devices with the CSMEs showed highly-stability in air at room temperature. These findings demonstrate that employing alcohol-soluble small molecule conjugated electrolyte is also a promising strategy to fabricate high-performance solution-processed PSCs, specifically for printable appropriate lower-band-gap active layer.

Supporting Information Available

The detailed experimental sections and the other characterization of devices are in

Supporting Information. This information is available free of charge via the Internet at <http://pubs.rsc.org/>.

Acknowledgements

The financial supports for this work are provided by the National Natural Science Foundation of China (51273088, and 51302130), National Basic Research Program of China (973 Program 2014CB260409), National Science Fund for Distinguished Young Scholars and Doctoral Programs Foundation of Ministry of Education of China (Grants 20133601110004 and 20133601120006). Yueqin Shi and Licheng Tan contributed equally to this work.

References:

1. Z. C. He, C. M. Zhong, S. J. Su, M. Xu, H. B. Wu, Y. Cao, *Nat. Photonics*, 2012, **6**, 591.
2. J. B. You, L. T. Dou, K. Yoshimura, T. Kato, K. Ohya, T. Moriarty, K. Emery, C. C. Chen, J. Gao, G. Li, Y. Yang, *Nat. Commun.*, 2013, **4**, 1446.
3. Z. He, C. Zhang, X. Xu, L. Zhang, L. Huang, J. Chen, H. Wu, Y. Cao, *Adv. Mater.*, 2011, **23**, 3086.
4. L. Dou, J. You, J. Yang, C.-C. Chen, Y. He, S. Murase, T. Moriarty, K. Emery, G. Li, Y. Yang, *Nat. Photonics*, 2012, **6**, 180.
5. W. Li, A. Furlan, K. H. Hendriks, M. M. Wienk, R. A. J. Janssen, *J. Am. Chem. Soc.*, 2013, **135**, 5529.
6. Y. Wu, S. E. Potts, P. M. Hermkens, H. C. M. Knoop, F. Roozeboom, W. M. M. Kessels, *Chem. Mater.*, 2013, **25**, 4619.
7. Y. Wang, X. Xin, Y. Lu, T. Xiao, X. Xu, N. Zhao, X. Hu, B. S. Ong, S. C. Ng, *Macromolecules*, 2013, **46**, 9587.
8. M.-H. Liao, C.-E. Tsai, Y.-Y. Lai, F.-Y. Cao, J.-S. Wu, C.-L. Wang, C.-S. Hsu, I. Liao, Y.-J. Cheng, *Adv. Funct. Mater.*, 2014, **24**, 1418.
9. K. H. Lee, P. E. Schwenn, A. R. G. Smith, H. Cavaye, P. E. Shaw, M. James, K. B. Krueger, I. R. Gentle, P. Meredith, P. L. Burn, *Adv. Mater.*, 2011, **23**, 766.

10. T. K. An, H. Kang, H.-J. Yun, H. Cha, J. Hwang, S. Park, J. Kim, Y. J. Kim, D. S. Chung, S.-K. Kwon, Y.-H. Kim, C. E. Park, *Adv. Mater.*, 2013, **25**, 7003.
11. A. T. Yiu, P. M. Beaujuge, O. P. Lee, C. H. Woo, M. F. Toney, J. M. J. Fréchet, *J. Am. Chem. Soc.*, 2012, **134**, 2180.
12. Z. He, C. Zhong, S. Su, M. Xu, H. Wu, Y. Cao, *Nat. Photonics*, 2012, **6**, 591.
13. H. Zhou, Y. Zhang, C.-K. Mai, S. D. Collins, T.-Q. Nguyen, G. C. Bazan, A. J. Heeger, *Adv. Mater.*, 2014, **26**, 780.
14. T. Yang, M. Wang, C. Duan, X. Hu, L. Huang, J. Peng, F. Huang, X. Gong, *Energy Environ. Sci.*, 2012, **5**, 8208.
15. J. Liu, M. Durstock, L. Dai, *Energy Environ. Sci.*, 2014, **7**, 1297.
16. H. L. Yip, A. K. Y. Jen, *Energy Environ. Sci.*, 2012, **5**, 5994.
17. R. Po, C. Carbonera, A. Bernardi, N. Camaioni, *Energy Environ. Sci.*, 2011, **4**, 285.
18. J. Liu, Y. Xue, Y. Gao, D. Yu, M. Durstock, L. Dai, *Adv. Mater.*, 2012, **24**, 2228.
19. L. Wang, H. Liu, R. M. Konik, J. A. Misewich, S. S. Wong, *Chem. Soc. Rev.*, 2013, **42**, 8134.
20. H. Chen, Y. Guo, G. Yu, Y. Zhao, J. Zhang, D. Gao, H. Liu, Y. Liu, *Adv. Mater.*, 2012, **24**, 4618.
21. F. Liu, Y. Gu, C. Wang, W. Zhao, D. Chen, A. L. Briseno, T. P. Russell, *Adv. Mater.*, 2012, **24**, 3947.
22. W. Shin, T. Yasuda, G. Watanabe, Y. S. Yang, C. Adachi, *Chem. Mater.*, 2013, **25**, 2549.
23. J. Mei, K. R. Graham, R. Stalder, S. P. Tiwari, H. Cheun, J. Shim, M. Yoshio, C. Nuckolls, B. Kippelen, R. K. Castellano, J. R. Reynolds, *Chem. Mater.*, 2011, **23**, 2285.
24. S. Loser, B. Valle, K. A. Luck, C. K. Song, G. Ogien, M. C. Hersam, K. D. Singer, T. J. Marks, *Adv. Energy Mater.*, 2014, 10.1002/aenm.201301938.
25. C. Kanimozhi, N. Yaacobi-Gross, K. W. Chou, A. Amassian, T. D. Anthopoulos, S. Patil, *J. Am. Chem. Soc.*, 2012, **134**, 16532.
26. Y. Li, P. Sonar, L. Murphy, W. Hong, *Energy Environ. Sci.*, 2013, **6**, 1684.

27. H. Bronstein, Z. Chen, R. S. Ashraf, W. Zhang, J. Du, J. R. Durrant, P. S. Tuladhar, K. Song, S. E. Watkins, Y. Geerts, M. M. Wienk, R. A. J. Janssen, T. Anthopoulos, H. Sirringhaus, M. Heeney, I. McCulloch, *J. Am. Chem. Soc.*, 2011, **133**, 3272.
28. K. M. O'Malley, C.-Z. Li, H.-L. Yip, A. K.-Y. Jen, *Adv. Energy Mater.*, 2012, **2**, 82.
29. Y. Lin, L. Ma, Y. Li, Y. Liu, D. Zhu, X. Zhan, *Adv. Energy Mater.*, 2013, **3**, 1166.
30. W. Ma, C. Yang, X. Gong, K. Lee, A. J. Heeger, *Adv. Funct. Mater.*, 2005, **15**, 1617.
31. F. Liu, Z. A. Page, V. V. Duzhko, T. P. Russell, T. Emrick, *Adv. Mater.*, 2013, **25**, 6868.
32. Z. A. Page, V. V. Duzhko, T. Emrick, *Macromolecules*, 2013, **46**, 344.
33. S. Zhong, R. Wang, H. Y. Mao, Z. He, H. Wu, W. Chen, Y. Cao, *J. Appl. Phys.*, 2013, **114**, 113709.
34. Y. Yuan, T. J. Reece, P. Sharma, S. Poddar, S. Ducharme, A. Gruverman, Y. Yang, J. Huang, *Nat. Mater.*, 2011, **10**, 296.
35. G. Zhao, Y. He, Z. Xu, J. Hou, M. Zhang, J. Min, H.-Y. Chen, M. Ye, Z. Hong, Y. Yang, Y. Li, *Adv. Funct. Mater.*, 2010, **20**, 1480.
36. Y. Liu, X. Wan, F. Wang, J. Zhou, G. Long, J. Tian, Y. Chen, *Adv. Mater.*, 2011, **23**, 5387.
37. Y.-J. Cheng, C.-H. Hsieh, P.-J. Li, C.-S. Hsu, *Adv. Funct. Mater.*, 2011, **21**, 1723.
38. K. Tremel, F. S. U. Fischer, N. Kayunkid, R. D. Pietro, R. Tkachov, A. Kiriy, D. Neher, S. Ludwigs, M. Brinkmann, *Adv. Energy Mater.*, 2014, 10.1002/aenm.201301659.
39. C.-Y. Mei, L. Liang, F.-G. Zhao, J.-T. Wang, L.-F. Yu, Y.-X. Li, W.-S. Li, *Macromolecules*, 2013, **46**, 7920.
40. Y. Sun, J. H. Seo, C. J. Takacs, J. Seifert, A. J. Heeger, *Adv. Mater.*, 2011, **23**, 1679.
41. C. E. Small, S. Chen, J. Subbiah, C. M. Amb, S.-W. Tsang, T.-H. Lai, J. R. Reynolds, F. So, *Nat. Photonics*, 2012, **6**, 115.

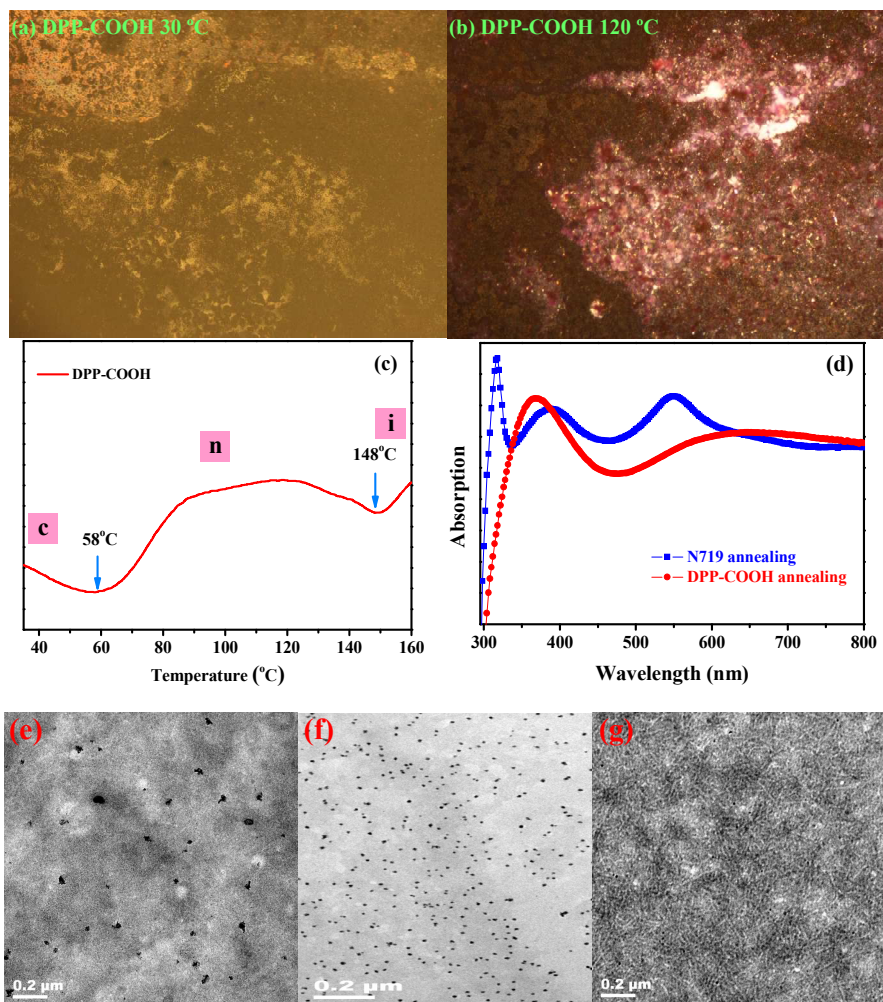


Fig. 1. Polarizing optical micrographs of DPP-COOH (a) at room temperature and (b) at 120 °C within anisotropic melt; (c) Differential scanning calorimetry thermogram of the DPP-COOH recorded under nitrogen at a scan rate of 20 °C/min; (d) UV-vis absorption spectra of DPP-COOH and N719 films as-spun from CH₃OH solution. Transmission electron microscopy (TEM) images of (e) pristine P3HT:PCBM film; (f) N719 on the top of pristine P3HT:PCBM film as HTL; (g) DPP-COOH on the top of pristine P3HT:PCBM film as HTL.

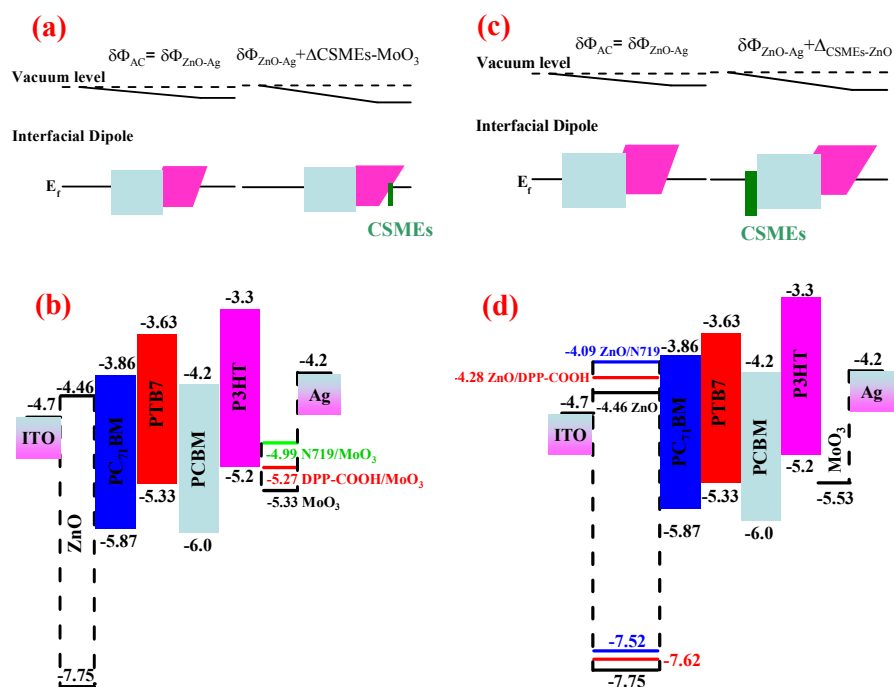


Fig. 2. (a) Schematic illustration of the built-in potential difference in device without (left) and with (right) a CSMEs interlayer as HTL, given for a common Fermi level (E_f) alignment; (b) Energy diagram of small molecules sandwich in between active layer and MoO_3 as hole transport layer. (c) Schematic illustration of the built-in potential difference in device without (left) and with (right) a CSMEs interlayer as ETL, given for a common Fermi level (E_f) alignment; (d) Energy diagram of small molecules sandwich in between active layer and ZnO as ETL.

Table 1. The device performance parameters of P3HT:PCBM and PTB7:PC₇₁BM inverted solar cells with different HTLs between active layer and MoO₃.

Device ^{a,b}	J_{sc} (mA/cm ²)	V_{oc} (V)	FF (%)	PCE (%)	R_s	R_{sh}
ITO/ZnO/PP ^c /MoO ₃ ^d /Ag	8.31	0.59	59	2.9±0.1	1.0	240.1
ITO/ZnO/PP ^c /N719/MoO ₃ ^d /Ag	9.47	0.57	50	2.7±0.2	5.3	1133.2
ITO/ZnO/PP ^c /N719 ^c /MoO ₃ ^d /Ag	9.24	0.58	58	3.1±0.2	1.0	1337.8
ITO/ZnO/PP ^c /DPP-COOH/MoO ₃ ^d /Ag	8.92	0.59	48	2.6±0.2	1.9	171.4
ITO/ZnO/PP ^c /DPP-COOH ^c /MoO ₃ ^d /Ag	8.86	0.58	57	3.0±0.2	1.2	361.7
ITO/ZnO/PTP ^c /MoO ₃ ^d /Ag ^f	14.60	0.72	64	6.7	11.5	332
ITO/ZnO/PTP ^c /N719/MoO ₃ ^d /Ag ^f	16.76	0.72	60	7.2	5.8	232
ITO/ZnO/PTP ^c /DPP-COOH/MoO ₃ ^d /Ag ^f	16.24	0.72	65	7.6	2.4	454

^a All values represented averages from fifteen 0.04 cm² devices on a single chip and the device area had been recollected. ^b Device structure: ITO:ZnO (20 nm)/active layer/Ag (MoO₃). ^c The devices were annealed at 150 °C for 10 min before anode electrode (Ag or MoO₃/Ag) evaporation. PP represented P3HT:PCBM (1:1 w/w) with thermal annealing at 150 °C for 10 min and PTP represented PTB7:PC₇₁BM (1:1.5 w/w, 3% DIO additive). ^d It presented 6 nm MoO₃ deposited on active layer surface. ^e It presented the thermal annealing treatments at 120 °C for 10 min after small molecules spin-coated onto the active layer surface. ^f Represented the best device performance parameters.

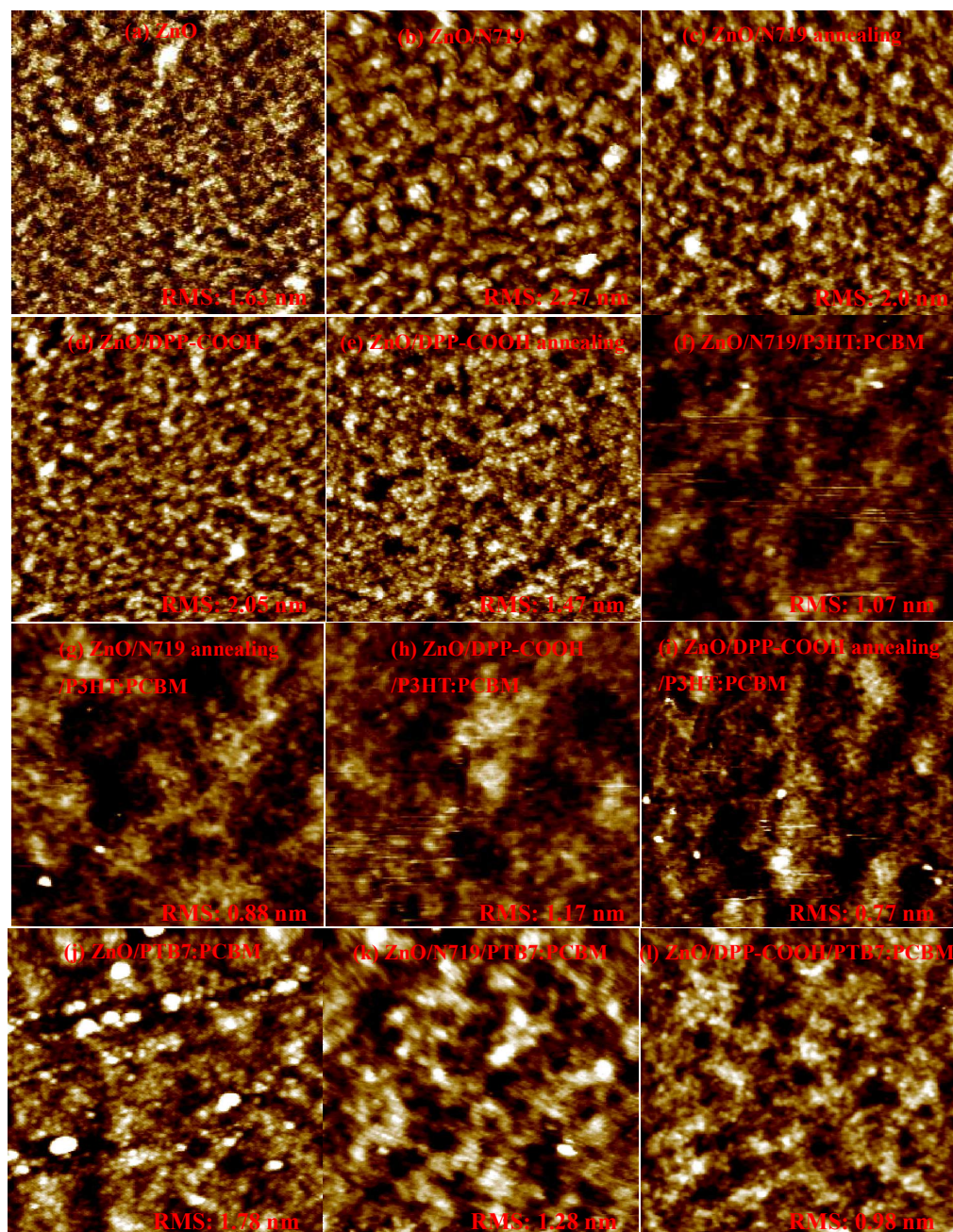


Fig. 3. Tapping-mode atomic force microscopy (AFM) high images of (a) the surface of pristine ZnO thin film, (b) the surface of ZnO/N719 thin film, (c) the surface of ZnO/N719 thin film with thermal annealing treatment, (d) the surface of ZnO/DPP-COOH thin film and (e) the surface of ZnO/DPP-COOH thin film with thermal annealing treatment. Height-mode AFM images of P3HT:PCBM on the top of different thin films of (f) ZnO/N719 thin film (g) ZnO/N719 thin film with thermal annealing treatment, (h) ZnO/DPP-COOH thin film and (i) ZnO/DPP-COOH thin

film with thermal annealing treatment. Height-mode AFM images of PTB7:PC₇₁BM on the top of (j) ZnO thin film, (k) ZnO/N719 thin film with thermal annealing at 120 °C for 10 min and (l) ZnO/DPP-COOH thin film with thermal annealing at 120 °C for 10 min. The image sizes were all 5 μm × 5 μm.

Table 2. Device parameters of P3HT:PCBM and PTB7:PC₇₁BM solar cells with different ETLs between active layer and ZnO.

Device ^{a,b}	J_{sc} (mA/cm ²)	V_{oc} (V)	FF (%)	PCE (%)	R_s	R_{sh}
ITO/ZnO/N719/PP ^c /MoO ₃ /Ag	8.57	0.62	65	3.5±0.2	5.9	1153
ITO/ZnO/N719 ^d /PP ^c /MoO ₃ /Ag	9.55	0.62	61	3.6±0.2	1.9	725.4
ITO/ZnO/DPP-COOH/PP ^c /MoO ₃ /Ag	8.03	0.60	63	3.0±0.2	6.9	552
ITO/ZnO/DPP-COOH ^d /PP ^c /MoO ₃ /Ag	9.19	0.62	61	3.5±0.2	9.0	1137
ITO/ZnO/N719/PTP ^c /MoO ₃ /Ag	15.29	0.74	66	7.4±0.2	1.7	398
ITO/ZnO/N719 ^d /PTP ^c /MoO ₃ /Ag	15.92	0.73	66	7.6±0.2	1.6	630
ITO/ZnO/DPP-COOH/PTP ^c /MoO ₃ /Ag	15.44	0.73	66	7.3±0.2	1.7	683
ITO/ZnO/DPP-COOH ^d /PTP ^c /MoO ₃ /Ag	16.01	0.74	67	8.0±0.2	1.5	563

^a All values represented averages from fifteen 0.04 cm² devices on a single chip and the device area had been recollected. ^b Device structure: ITO/ZnO (20 nm)/active layer/Ag (6.0 nm MoO₃). ^c PP represented P3HT:PCBM (1:1 w/w) with thermal annealing at 150 °C for 10 min before anode electrode (Ag or MoO₃/Ag) evaporation and PTP represented PTB7:PC₇₁BM (1:1.5 w/w). ^d It presented the thermal annealing treatments at 120 °C for 10 min after small molecules spin-coated on ZnO surface.

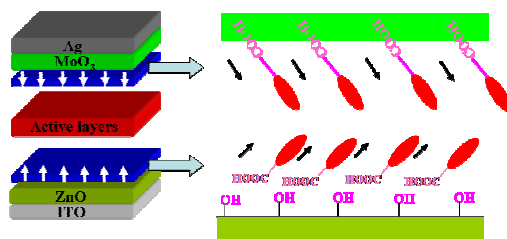
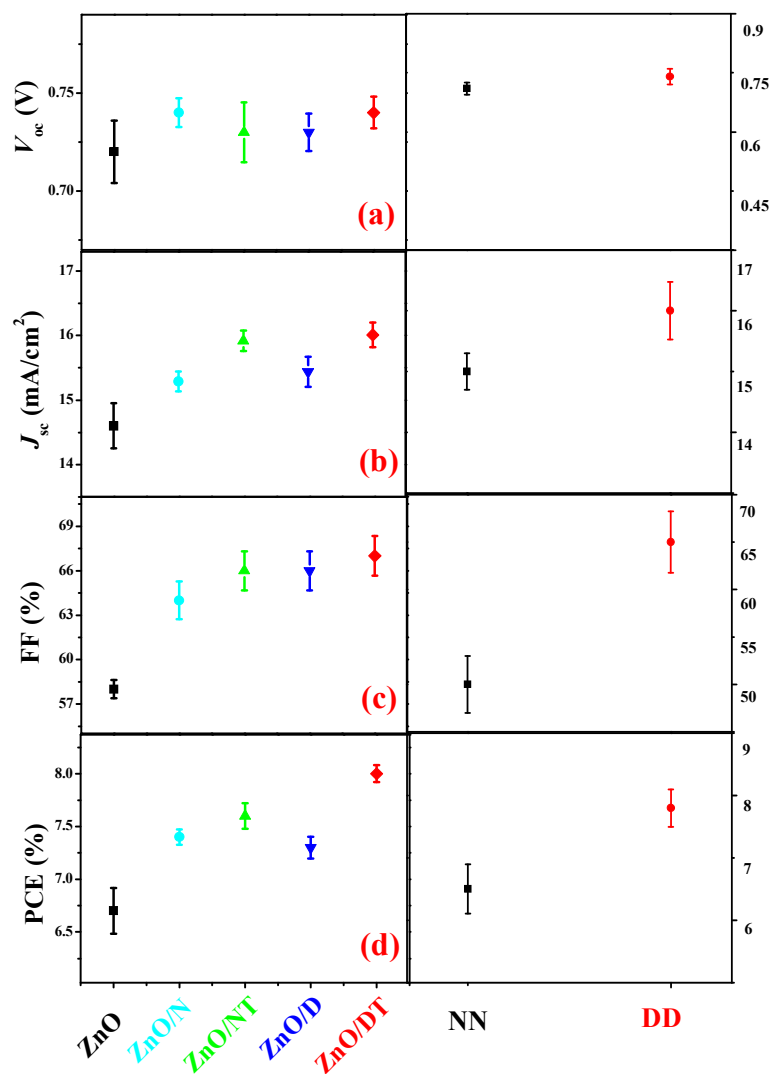


Fig. 4. Summary of device performance with different ETLs for (a) open-circuit voltage; (b) short-circuit current density; (c) fill factor; and (d) power conversion efficiency. The ZnO cathode interlayer is shown for reference. The N and NT represent N719 without and with the thermal annealing treatment at 120 °C for 10 min after small molecules spin-coated on ZnO surface; The D and DT represent

DPP-COOH without and with the thermal annealing treatment at 120 °C for 10 min after small molecules spin-coated on ZnO surface. Summary of device performance with CSMEs as ETL and HTL simultaneously, the NN represents the device with N719 as the HTL and ETL and DD represents the device with DPP-COOH as the HTL and ETL simultaneously. The inset is schematic representations of the spontaneous dipole moment orientation induced by adding CSMEs as ETL and HTL simultaneously.

Highlights

Alternative Alcohol-soluble Conjugated Small Molecule Electrolytes for High-efficiency Inverted Polymer Solar Cells

Yueqin Shi, Licheng Tan, Lie Chen, Yiwang Chen*

Alcohol-soluble small molecule conjugated electrolytes are utilized as both hole and electron transport interlayer simultaneously in inverted polymer solar cells.

Graphical abstract

